Supplementary Material: Collective Motion and Its Connection to the Energy Landscape in 2D Soft Crystals

Md. Rakib Hassan,[a] Sam R. Aronow,[a] Jack F. Douglas,[b] and Francis W. Starr[a]

[a] *Physics Department, Wesleyan University, Middletown, CT 06459, USA*

[b] *Materials Science and Engineering Division, National Institute of Standards and Technology, Gaithersburg, MD, 20899, USA*

The data shown are generally all from the dusty plasma crystal (DPC); the data from the colloidal crystal show the same qualitative features, though packing fraction plays the role of temperature in that case.

DYNAMIC PROPERTIES

Mean Square Displacement $< r^2 >$

The mean square displacement $< r^2 >$ of the dusty plasma crystal (DPC) is plotted across a range of temperatures in Fig. S1. The plot clearly illustrates three distinct timescales, each corresponding to different types of dust particle dynamics. In the initial timescale, specifically for the dimensionless time range $t \leq 10$, particles exhibit ballistic motion, and their displacement in time appears to be nearly independent of temperature. Moving on to an intermediate timescale, the set of curves at lower temperatures (associated with solid and hexatic phases) indicates particle caging, associated with intermittent particle motions when individual particles are observed. As the temperature decreases, the particles find it increasingly caged, hindering the onset of the diffusion process. At longer timescales, the system transitions into a linear variation of $< r^2 >$ with time, corresponding to diffusive motion. In the case of the fluid phase, there is no intermediate caging regime – particles start diffusing right after a transient ballistic regime. For the colloidal system, the same qualitative behavior occurs when packing fraction is varied, rather than temperature.

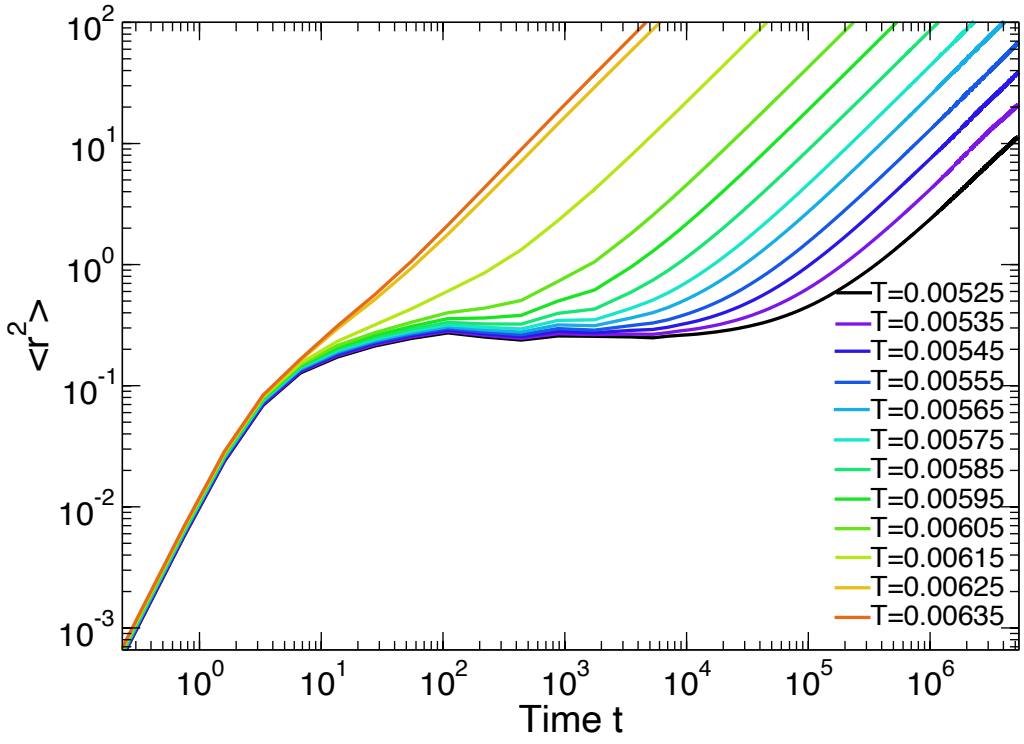

S1. Mean-square-displacement $< r^2 >$ plotted for different temperatures suggesting different phases of matter: solid, hexatic, and fluid.

Non-Gaussian Parameter

The extent of deviation in particle displacement distribution from a Gaussian distribution is quantified by the non-Gaussian parameter:

$$\alpha_2(t) = \frac{1}{2}\frac{\langle(\Delta r(t))^4\rangle}{[\langle(\Delta r(t))^2\rangle]^2} - 1. \tag{1}$$

As depicted in Fig. S2, the displacement distributions for the DPC tend to be nearly Gaussian at short timescales and gradually approach Gaussian behavior at very long timescales, as $\alpha_2 \to 0$. However, on intermediate timescales, a distinct and well-defined timescale, characterized as the characteristic timescale t^*, emerges for each temperature. This timescale, illustrated in Fig. 12, exhibits an increase with temperature-dependent rather than the decrease generally observed in glass-forming liquids. Curiously, the magnitude of the α_2 (t^*) appears to be non-monotonic with temperature. During this intermediate timescale, the system manifests its most non-Gaussian behavior.

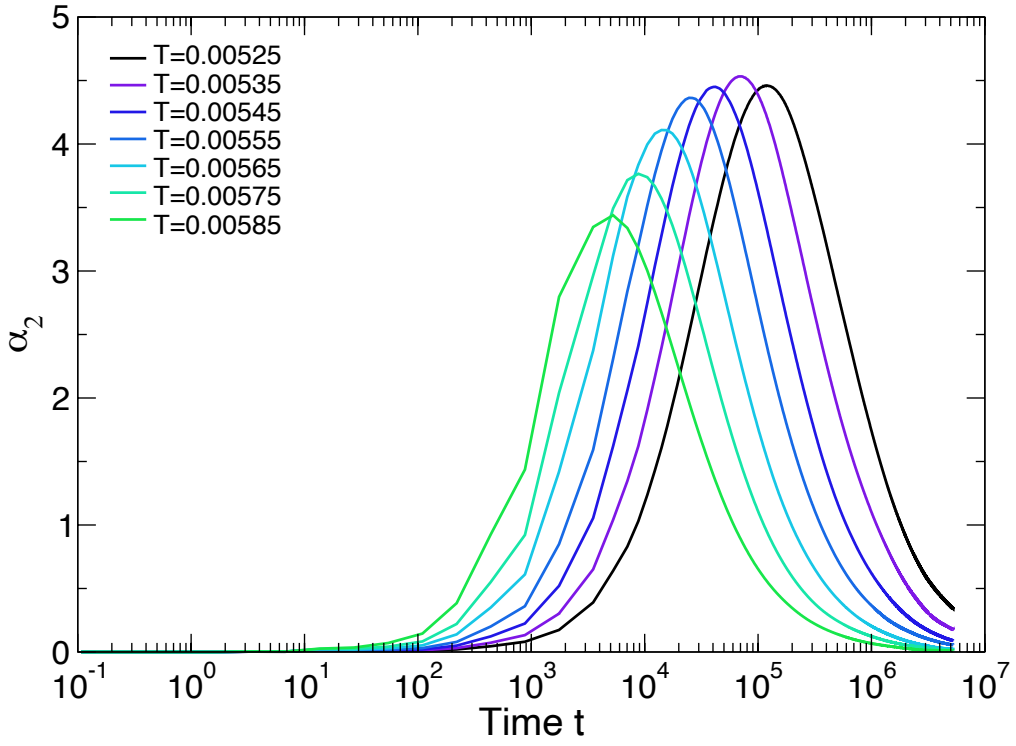

S2. Variation of the non-Gaussian parameter for various temperatures of the DPC.

Self Intermediate Scattering Function $F_s(q_0, t)$

The self intermediate scattering function (SISF) $F_s(q_0, t)$ is commonly used to quantify single-particle dynamics and is defined as,

$$F_s(q_0, t) = \frac{1}{N} \left\langle \sum_{i=1}^{N} \exp(-i\mathbf{q_0} \cdot (\mathbf{r}_i(t) - \mathbf{r}_i(0))) \right\rangle . \tag{2}$$

The plot in Fig. S3 for the DPC mirrors the distinct timescales of particle dynamics observed in the mean square displacement plot. This graphical representation also unveils two distinct relaxations: the short-time β relaxation and the long-time α relaxation linked to diffusive motion and the equilibration of the material on long timescales. The characteristic relaxation time τ of $F_s(q_0, t)$ is obtained by fitting the α-relaxation to a stretched exponential function.

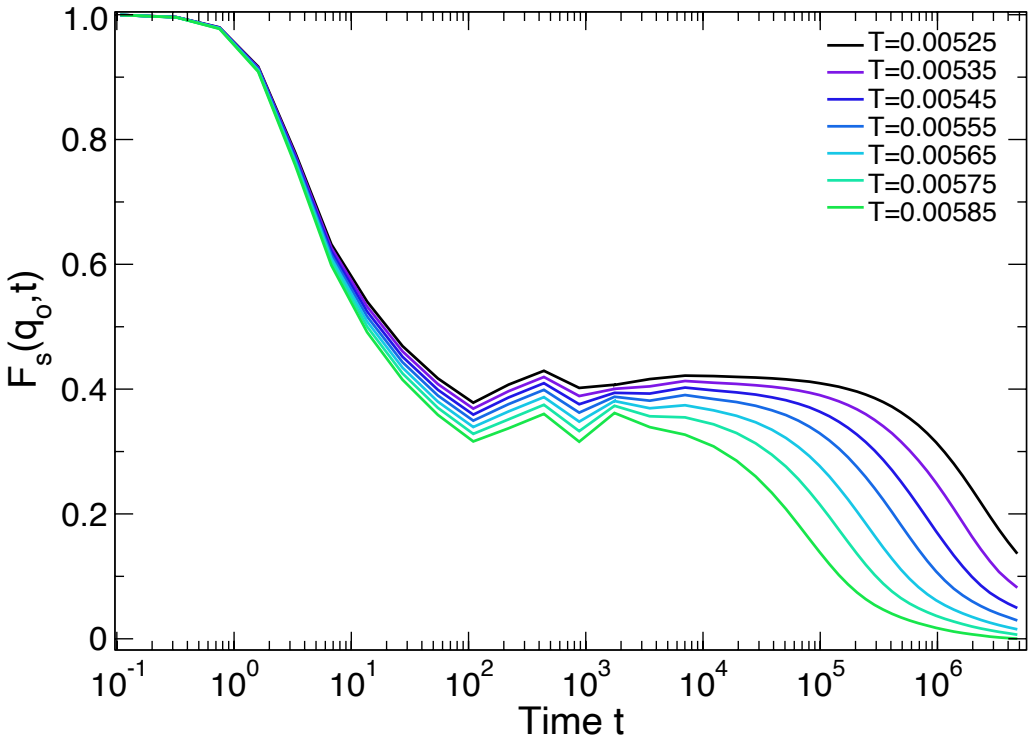

S3. Self part of the intermediate scattering function of the DPC for different temperatures confirms different types of particle dynamics in three distinct timescales as the mean square displacement plot.

Parametric Plot of Characteristic Timescales

For the DPC, all the characteristic timescales (relaxation time τ-black, time to reach maximum non-Gaussian parameter t^*-red, and diffusive timescale $(D/T)^{-1}$-green) discussed in the paper are plotted in Fig. S4 against the ground state timescale $t_{\rm gr}$ at different temperatures. The functional dependencies are also mentioned, along with the corresponding fits. It is clear from the plots that t^* and $t_{\rm gr}$ are linearly dependent on each other, whereas τ and $(D/T)^{-1}$ are very weakly nonlinear, both with a coupling exponent 1.08; the fact that both have the same exponent implies a linear relation between τ and $(D/T)^{-1}$. In the inset, the same timescales are normalized by $t_{\rm gr}$ and then plotted at different temperatures. This shows that t_gr remains nearly constant at different temperatures, suggesting these two timescales track each other. However, τ and $(D/T)^{-1}$ both decrease in a similar fashion upon heating the crystal.

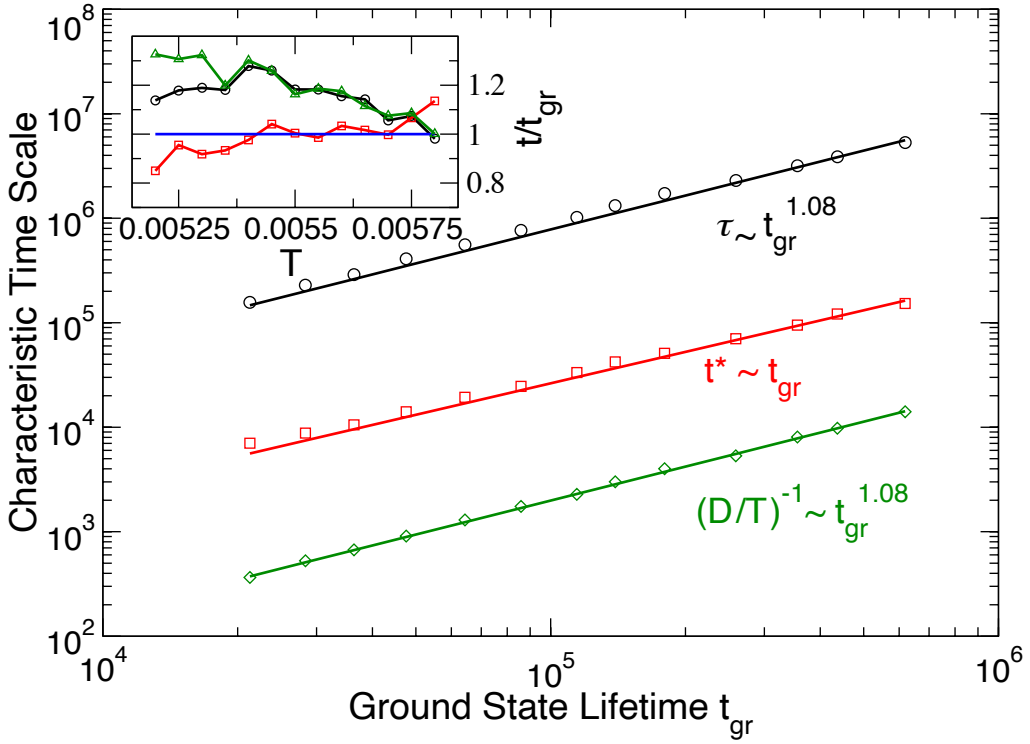

S4. Parametric plot of different timescales of dynamics in DPC with inset showing a week decoupling effect.

Defects in Real and IS Trajectories

In the real trajectory, both stable and unstable defects coexist, whereas in the IS trajectory, only the stable defects persist (by definition). Consequently, the real trajectory naturally exhibits a higher number of defects compared to the IS trajectory. Fig. S5 illustrates a comparison of the defect cluster counts between these two trajectories for the DPC. It is evident from this plot that it is impossible to differentiate between the ground state and excited states by simply looking at the real trajectory time series data.

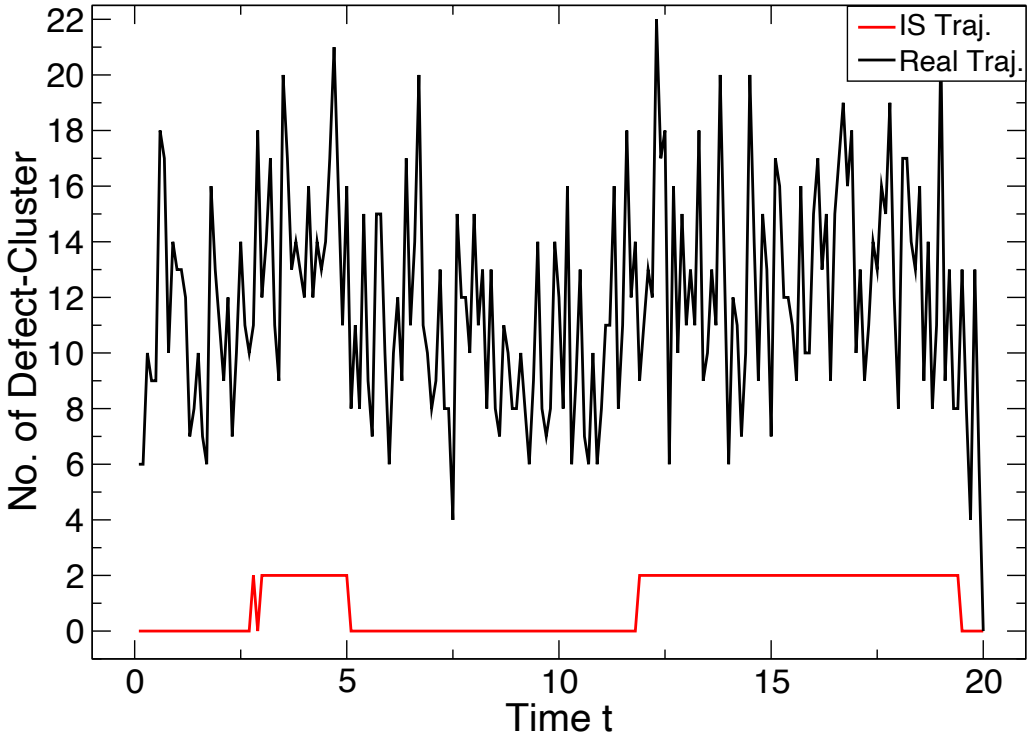

S5. The number of defect-cluster in IS trajectory with the corresponding real trajectory in DPC.

As noted in the main manuscript, stable and unstable defects in the instantaneous configuration can largely be distinguished from their structure. Figure S6 shows that unstable defects are predominantly observed as two 5-7 defect pairs arranged in a nearly square configuration. Similar visualizations of stable and unstable defects have also been reported by Qi et al. [1].

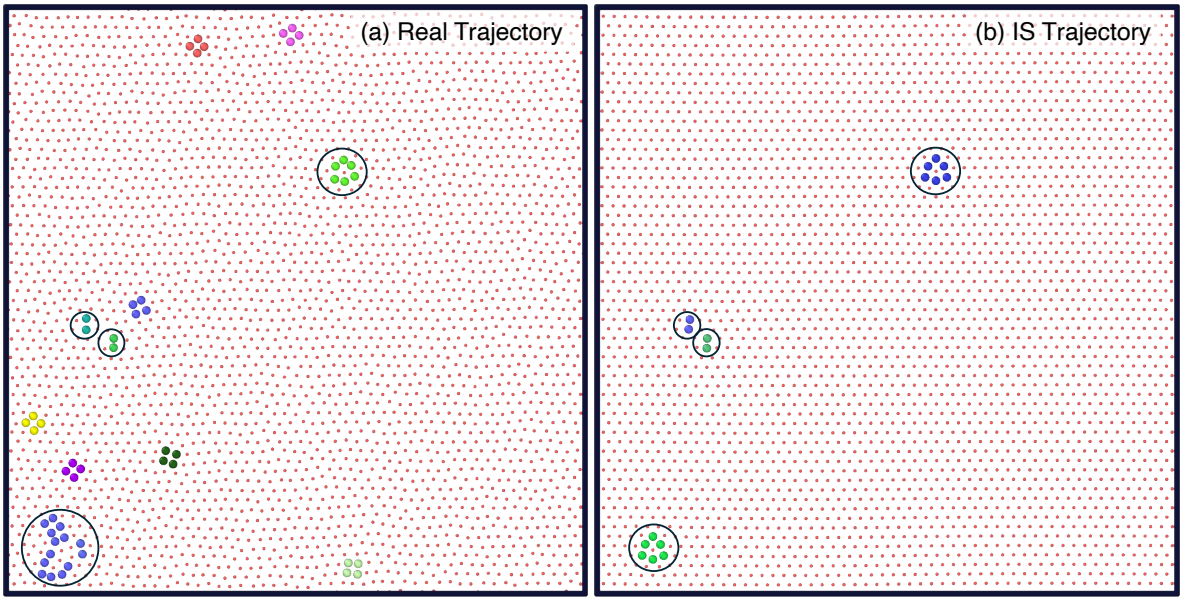

S6. Visualization of defect clusters in (a) a real (instantaneous) configuration and (b) an inherent structure (IS) configuration. Only stable defects are circled to distinguish them from unstable defects. Both panels were rendered using OVITO [2].

Defect Cluster Size

In the colloidal crystal, nearly all defect clusters are size 6 (three 5-7 defect pairs), where vacancies feature a 6-membered ring with a hole in the middle, and interstitials have an extra (non-defect) particle at the center of the ring. As discussed in the main text, the situation is more complex in the DPC where there are no core interactions. Fig. S7 shows that most defects are created in pairs of clusters of size 6 and 4 (two 5-7 defect pairs); in this case, clusters of size 6 are predominantly interstitials while clusters of size 4 are predominantly vacancy clusters. As the figure illustrates, vacancy clusters in the DPC do not exhibit an explicit hole, but are simply locally less dense. In addition, the DPC also features a non-trivial fraction of clusters of size 3 (one 5-8-5 defect string) and dipoles of a single 5-7 defect pair.

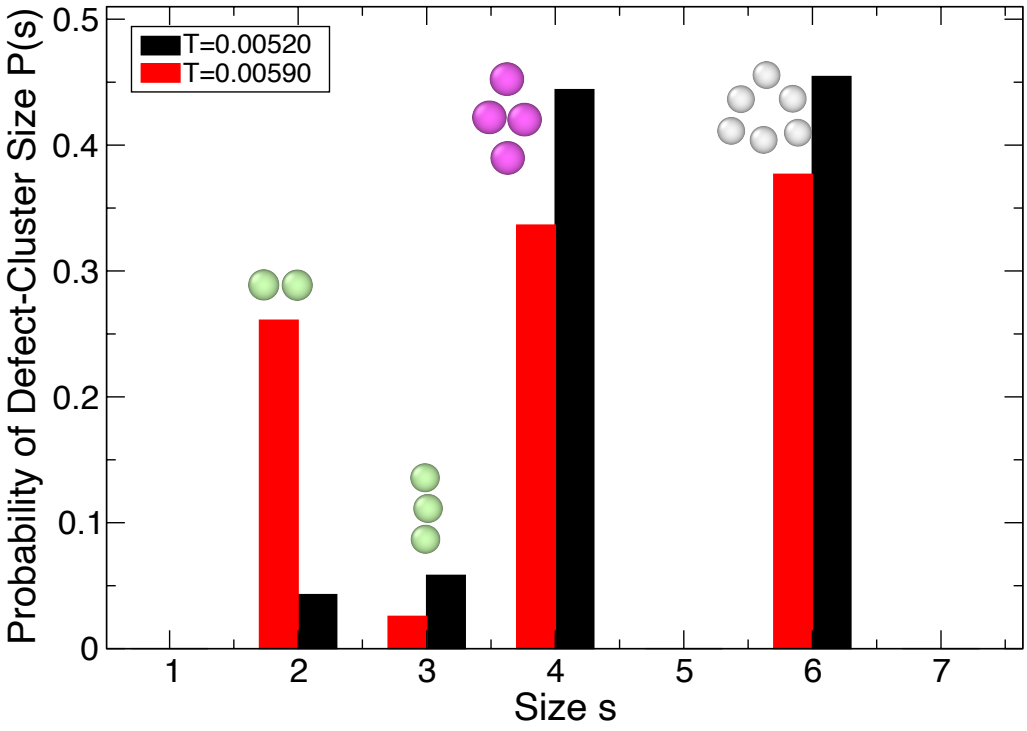

S7. Probability distribution of defect cluster size at a low ($T = 0.0052$) and high ($T = 0.0059$) temperatures in the DPC. The dominant contribution at low T are clusters of size 4 and 6; dipoles play an increasingly important role as melting is approached. The figure also show illustrations of typical clusters of each size. The cluster of size 4 is an interstitial (relatively higher density) while the cluster of size 6 is a vacancy (relatively low density with a gap in the middle). These are just examples, as clusters of each size can be interstitials or vacancies.

REFERENCES

[1] W.-K. Qi, Z. Wang, Y. Han, and Y. Chen, The Journal of Chemical Physics **133**, 234508 (2010).

[2] A. Stukowski, Modelling and simulation in materials science and engineering **18**, 015012 (2010).